Autosomal Recessive Bestrophinopathy Is Not Associated With the Loss of Bestrophin-1 Anion Channel Function in a Patient With a Novel *BEST1* Mutation

Adiv A. Johnson,[1] Lori A. Bachman,[1] Benjamin J. Gilles,[1] Samuel D. Cross,[1] Kimberly E. Stelzig,[2] Zachary T. Resch,[2] Lihua Y. Marmorstein,[1] Jose S. Pulido,[1,3] and Alan D. Marmorstein[1]

[1]Department of Ophthalmology, Mayo Clinic, Rochester, Minnesota, United States
[2]Center for Regenerative Medicine, Mayo Clinic, Rochester, Minnesota, United States
[3]Department of Molecular Medicine, Mayo Clinic, Rochester, Minnesota, United States

Correspondence: Alan D. Marmorstein, Department of Ophthalmology, Mayo Clinic, 200 1st Street SW, Rochester, MN 55905, USA; Marmorstein.Alan@mayo.edu.
Jose S. Pulido, Department of Ophthalmology, Mayo Clinic, 200 1st Street SW, Rochester, MN 55905, USA;
Pulido.Jose@mayo.edu.

Submitted: March 19, 2015
Accepted: June 4, 2015

Citation: Johnson AA, Bachman LA, Gilles BJ, et al. Autosomal recessive bestrophinopathy is not associated with the loss of bestrophin-1 anion channel function in a patient with a novel *BEST1* mutation. *Invest Ophthalmol Vis Sci*. 2015;56:4619–4630. DOI:10.1167/iovs.15-16910

Purpose. Mutations in *BEST1*, encoding bestrophin-1 (Best1), cause autosomal recessive bestrophinopathy (ARB). Encoding bestrophin-1 is a pentameric anion channel localized to the basolateral plasma membrane of the RPE. Here, we characterize the effects of the mutations R141H (CGC > CAC) and I366fsX18 (c.1098_1100+7del), identified in a patient in our practice, on Best1 trafficking, oligomerization, and channel activity.

Methods. Currents of Cl^- were assessed in transfected HEK293 cells using whole-cell patch clamp. Best1 localization was assessed by confocal microscopy in differentiated, human-induced pluripotent stem cell-derived RPE (iPSC-RPE) cells following expression of mutants via adenovirus-mediated gene transfer. Oligomerization was evaluated by coimmunoprecipitation in iPSC-RPE and MDCK cells.

Results. Compared to Best1, $Best1^{I366fsX18}$ currents were increased while $Best1^{R141H}$ Cl^- currents were diminished. Coexpression of $Best1^{R141H}$ with Best1 or $Best1^{I366fsX18}$ resulted in rescued channel activity. Overexpressed Best1, $Best1^{R141H}$, and $Best1^{I366fsX18}$ were all properly localized in iPSC-RPE cells; $Best1^{R141H}$ and $Best1^{I366fsX18}$ coimmunoprecipitated with endogenous Best1 in iPSC-RPE cells and with each other in MDCK cells.

Conclusions. The first 366 amino acids of Best1 are sufficient to mediate channel activity and homo-oligomerization. The combination of Best1 and $Best1^{R141H}$ does not cause disease, while $Best1^{R141H}$ together with $Best1^{I366fsX18}$ causes ARB. Since both combinations generate comparable Cl^- currents, this indicates that ARB in this patient is not caused by a loss of channel activity. Moreover, $Best1^{I366fsX18}$ differs from Best1 in that it lacks most of the cytosolic C-terminal domain, suggesting that the loss of this region contributes significantly to the pathogenesis of ARB in this patient.

Keywords: Best1, iPSC-RPE, localization, oligomerization

Mutations in *BEST1* (NM_004183.3) have been reported to cause clinically distinct, inherited retinal degenerative disorders (http://www-huge.uni-regensburg.de/BEST1_database/home.php?select_db=BEST1), including Best vitelliform macular dystrophy[1,2] (BVMD) and autosomal recessive bestrophinopathy[3] (ARB). While Best vitelliform macular dystrophy is the most prevalent disease caused by *BEST1* mutation, ARB is the only bestrophinopathy characterized by a recessive mode of inheritance. Autosomal recessive bestrophinopathy causes significant vision loss and can be caused by either compound heterozygous or homozygous mutations in *BEST1*.[4,5] In ARB patients, the electrooculogram (EOG) is diminished and fundus findings include anomalous multifocal subretinal deposits, subretinal fluid accumulation, localized retinal detachment, and abnormal autofluorescence.[4,5] Age of onset varies considerably, but manifestation of disease has been reported to occur as early as 4 years of age.[4,5] Very little is known about the pathogenesis of ARB and, currently, no effective therapies exist for these patients.

The gene *BEST1* encodes for human bestrophin-1 (Best1), a 585-amino acid, 68-kD, integral membrane protein localized to the basolateral plasma membrane of the RPE.[6] Monomers of Best1 have four transmembrane domains as well as intracellular N- and C-termini, with the latter being at the terminus of a large, cytosolic domain.[7–9] Monomers of Best1 oligomerize[10–14] to form a highly conserved homopentameric Ca^{2+}-activated ion channel.[8,9] Data from heterologous systems,[15,16] primary human RPE cell culture,[17,18] mouse models,[19,20] the structurally similar paralog bestrophin-2,[21,22] as well as recently published crystal structures[8,9] all unambiguously demonstrate that mammalian Best1 is a calcium-activated anion channel. In addition to functioning as an anion channel, Best1 regulates intracellular Ca^{2+} signaling and influences Ca^{2+} homeostasis.[17,23–30] Disease-causing mutations have been shown to disrupt Best1 protein trafficking, channel activity,[10,11,17,31] and intracellular Ca^{2+} signaling.[16,17,24,26] Although it is not yet clear how or if disruption of these parameters results in disease, it is well established that Best1 influences ion flux and that disease-causing mutations can disrupt its ability to do so.

Here, we present a 14-year old female patient with ARB and compound heterozygous mutations in *BEST1*. One mutation, R141H, has been previously reported in association with ARB.[3,32] The other mutation, I366fsX18, is a novel frameshift mutation resulting from a deletion of 10 nucleotides (c.1098_1100+7del) spanning an intron/exon splice boundary that is predicted to result in an early stop codon. Although neither of this patient's parents exhibit symptoms of disease, she presents with decreased vision and clear evidence of retinal dysfunction. In addition to presenting this case clinically, we employed differentiated, human RPE cells derived from induced pluripotent stem cells (iPSC-RPE) to investigate the effects of these mutations on Best1 trafficking and oligomerization. Confluent, polarized Madin-Darby canine kidney II (MDCK) cells were also used to further assess mutant oligomerization independent of endogenous Best1. Anion channel activity of each mutant was assayed using whole-cell patch clamp in human embryonic kidney 293 (HEK293) cells.

Our data from the truncated Best1^{I366fsX18} mutant show that the first 366 amino acids are sufficient for channel activity and homo-oligomerization. We also show, for the first time, that two ARB mutants can physically interact with endogenous Best1 in a native system as well as with each other in a heterologous system. Our data suggest that diminished channel activity is not causally associated with ARB in this patient and that the absence of the C-terminus in the Best1^{I366fsX18} mutant significantly contributes to the disease phenotype. These data provide new insights into the pathogenesis of ARB as well as the protein regions governing channel activity and oligomerization of Best1.

Methods

Cell Culture, Plasmids, Transfections, and Replication-Defective Adenoviruses

We maintained HEK293 and MDCK II cells (American Type Culture Collection, Manassas, VA, USA) as previously described[10,11]: in a 95% air 5% CO_2 environment at 37°C. Transfections were carried out as before[10,11,17] using a commercial reagent (Lipofectamine; Invitrogen, Carlsbad, CA, USA).

With the exception of Best1^{I366fsX18}-CFP, all plasmids and viruses used have been described previously.[10,11] We synthesized the cDNA for the novel Best1 mutant synthetically (Integrated DNA Technologies, Coralville, IA, USA) and spliced into the NheI and AgeI restriction sites of pECFP-N1 (Clontech Laboratories, Inc., Mountain View, CA, USA) in-frame with CFP. To generate a replication-defective adenovirus encoding for this mutant fused to CFP, Best1^{I366fsX18}-CFP was spliced into the KpnI and XhoI restriction sites of the viral shuttle vector pacAd5CMVK-NpA (Gene Transfer Vector Core, University of Iowa, Iowa City, IA, USA). The Best1^{I366fsX18}-CFP virus was then generated, amplified, purified, and titrated by the Gene Transfer Vector Core at the University of Iowa.

iPSC-RPE Differentiation

We obtained induced pluripotent stem cells from the Mayo Clinic Center for Regenerative Medicine BioTrust (Rochester, MN, USA). The cell line 006-BIOTR-0001 was generated from skin fibroblasts donated by a patient with no known retinal disease. Chromosomal integrity, stem cell marker profiles, and pluripotency of iPSCs were all verified by the Mayo Clinic Center for Regenerative Medicine BioTrust. Induced pluripotent stem cells were differentiated into RPE according to the method of Maruotti et al.[33] For all immunofluorescence and biochemical experiments, differentiated RPE were grown on Transwell permeable supports with 0.4 μM polycarbonate membranes (Corning, Inc., Tewksbury, MA, USA) for ≥2 months.

Phagocytosis

Assays of photoreceptor outer segment (OS) phagocytosis by iPSC-RPE were performed as described previously[34] with the following modifications: iPSC-RPE grown on 96-well plates was incubated with bovine OS labeled with FITC for 0, 1, 2, 3, or 5 hours, after which they were washed with ice cold PBS containing 0.13 mM $CaCl_2$ and 1 mM $MgCl_2$ (PBS-CM). To determine the number of internalized versus total OS, half of the wells at each time point were incubated for 10 minutes with 0.2% trypan blue in PBS-CM to quench the fluorescence of OS that had not been internalized. Following a series of washes in PBS-CM, cells were fixed in 4% paraformaldehyde in PBS-CM, then washed in PBS-CM. Outer segment counts were made with a plate reader (SpectraMax i3; Molecular Devices, Sunnyvale, CA, USA) equipped with an imaging cytometer equipped with data acquisition and analysis software (MiniMax 300 and SoftMax Pro 6.4; Molecular Devices).

Whole-Cell Patch Clamp

Whole-cell patch clamp was performed as before.[17] Human embryonic kidney 293 cells were transfected with wild-type (WT) or mutant Best1 fused in frame with a CFP or YFP tag using transfection reagent (Invitrogen). Like we have done previously,[17] single cells were identified by CFP and/or YFP fluorescence and used for whole-cell patch clamp experiments 24 to 72 hours after transfection. Recordings were obtained using a conventional whole-cell patch clamp technique with an EPC-10 amplifier and software (Patchmaster; HEKA, Lambrecht/Pfalz, Germany). Resistances of fire-polished borosilicate glass patch pipettes were 3 to 5 MΩ and experiments were conducted at RT. Due to the liquid junction potentials being small and <2 mV, no correction was made. The high intracellular Ca^{2+} solution contained (in mM): 146 CsCl, 2 $MgCl_2$; 5 Ca^{2+}-EGTA (free Ca^{2+} ~20 μM); 10 HEPES; 10 sucrose, pH 7.3, adjusted with NMDG. The standard extracellular solution contained (in mM): 140 NaCl; 5 KCl; 2 $CaCl_2$; 1 $MgCl_2$; 15 glucose; 10 HEPES; pH 7.4 with NaOH. The combination of these solutions set E_{rev} for Cl^- currents to zero, while cation currents carried by Cs^+ or Na^+ had very negative or positive E_{rev}, respectively. Osmolarity was adjusted to 303 mOsm using sucrose for all solutions. The mean membrane capacitance of the cells patched was 13.1 ± 0.6 pF ($n = 115$).

Electron Microscopy

We fixed iPSC-RPE permeable inserts (Corning, Inc.) in 2% paraformaldehyde/2.5% glutaraldehyde in cacodylate buffer for 1 hour at 4°C. The samples were rinsed in cacodylate buffer, postfixed in 1% osmium tetroxide for 1 hr, rinsed with ddH_2O, dehydrated with ascending concentrations of ethanol, and embedded in Spurr resin overnight. 100 nm sections were cut, stained with uranyl acetate and lead citrate, and viewed with a Jeol 1400 transmission electron microscope (JEOL USA, Peabody, MA, USA).

Immunofluorescence Microscopy

Immunofluorescence was performed as described previously.[10,11,17] Immunofluorescence of filters (Transwell; Corning, Inc.) 48 hours after infection with specified adenovirus vectors was performed with the following modifications: a rabbit,

Investigative Ophthalmology & Visual Science

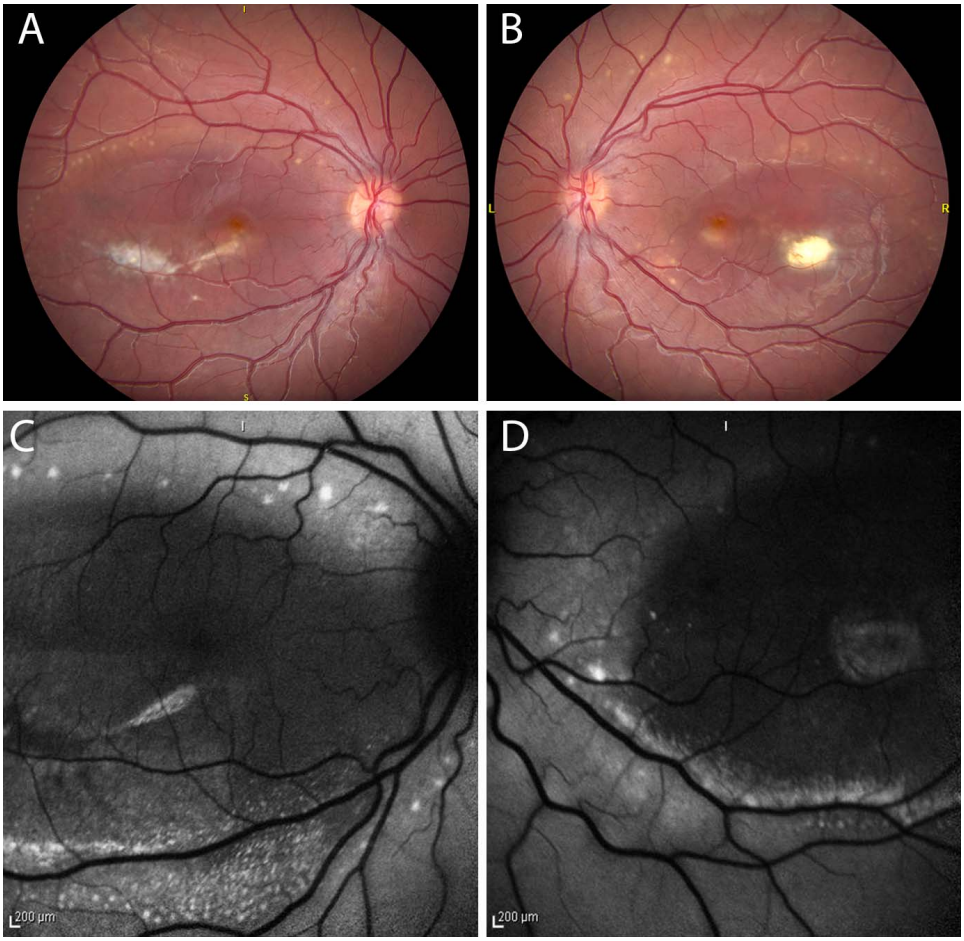

FIGURE 1. Fundus photographs and fundus autofluorescence in the affected patient. Fundus photographs of the patient's left (**A**, **C**) and right eyes (**B**, **D**) showing classical findings of ARB, including multifocal sub-RPE lesions and subretinal fibrosis (**A**, **B**). The sub-RPE lesions in both eyes were autofluorescent (**C**, **D**).

polyclonal antibody (Life Technologies, Frederick, MD, USA) was used to stain ZO-1 (1:100). We stained CFP and YFP using mouse, monoclonal (JL-8; Clontech Laboratories, Inc.) or rabbit, polyclonal (Clontech Laboratories, Inc.) antibodies to GFP at a dilution of 1:1000. We stained Best1 using either the rabbit, polyclonal antibody Pab-125 (1:1000) or the mouse, monoclonal antibody E6-6 (1:1000), both of which have been previously described.[6] Images were obtained using a ×40 Plan Apo oil immersion objective on a confocal microscope (C2; Nikon Instruments, Tokyo, Japan).

Immunoprecipitation and Western Blotting

Immunoprecipitation and Western blots were performed as described previously.[10,11] For immunoprecipitation and blotting of Best1, the rabbit, polyclonal Pab-125 and the mouse, monoclonal E6-6 were used, respectively. For immunoprecipitation and blotting of cellular retinaldehyde binding protein (CRALBP), a rabbit, polyclonal antibody (Novus Biologicals, Cambridge, UK) and a mouse, monoclonal antibody (ab15051; Abcam, Cambridge, UK) were used. For retinal pigment epithelium 65 and β-actin, the mouse, monoclonal antibody 8B11 (Santa Cruz Biotechnology, Dallas, TX, USA) and the mouse, monoclonal antibody AC-74 (Sigma-Aldrich Corp., St. Louis, MO, USA) were used, respectively. For CFP and YFP, we used the anti-GFP monoclonal antibody JL-8 (Clontech Laboratories, Inc.) or a rabbit anti-GFP polyclonal antibody (Clontech Laboratories, Inc.).

Statistics

Statistics were done using *t* tests. Significance was defined as $P < 0.05$.

RESULTS

Case Report

The subject is a 14-year-old female who was referred to our clinic at the age of 7 for a decrease in vision. At her initial exam, she presented with a visual acuity of 20/100 OD and 20/50 OS. She had accommodative esotropia and bilateral macular lesions with apparent multifocal sub-RPE lesions and subretinal fibrosis (Figs. 1A, 1B). The sub-RPE lesions were autofluorescent (Figs. 1C, 1D). Optical coherence tomography (OCT) revealed localized serous retinal detachments in both eyes with fibrotic mounds and irregular, elongated photoreceptor outer segments (Fig. 2). Her ratios of EOG Arden were ~1.1 in both eyes. As a result, genetic testing by the Carver Genetic Testing Lab at the University of Iowa was obtained which detected compound heterozygous mutations in *BEST1*. These mutations were R141H (CGC > CAC) and a novel, frameshift mutation I366fsX18 (c.1098_1100+7del). The mutations were confirmed using NextGen DNA sequencing at the Mayo Clinic Center for Individualized Medicine Gene Expression Core Facility. No

Investigative Ophthalmology & Visual Science

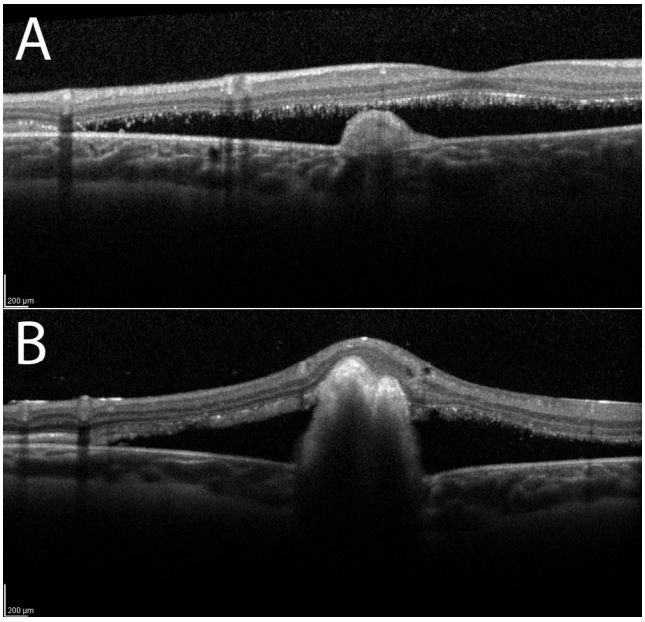

FIGURE 2. Optical coherence tomography imaging of the patient with autosomal recessive bestrophinopathy; OCT of a horizontal section of the macula demonstrates a serous retinal detachment present in both the right (**A**) and left (**B**) eyes. Small cysts of hyporeflective, intraretinal fluid were observed in the patient's left eye (**B**). In both the right (**A**) and left (**B**) eyes, outer segments appeared abnormally elongated, though this was especially pronounced in the right eye (**A**).

mutations were observed in a panel of 12 other genes known to cause inherited maculopathies.

Both clinical genetic testing and NextGen DNA sequencing revealed that the subject's father is a heterozygous carrier for the mutation R141H (CGC > CAC) and that the mother is a heterozygous carrier for the mutation I366fsX18 (c.1098_1100+7del). No mutations were identified in the mother or father in any other genes known to be associated with inherited maculopathies. No familial history of ophthalmic disease was indicated, and neither parent presented with an abnormal fundus (Figs. 3A, 3B). On the basis of the EOG, the appearance of the subject's fundus (Figs. 1, 3C); autofluorescence (Figs. 1C, 1D); OCT imaging (Fig. 2); and genetic testing, the subject was diagnosed with ARB at age 12. As of her last visit in November 2014, the subject's visual acuity had improved to 20/60 OD and 20/25 OS and the appearance of her fundus remained unchanged.

Effects of Mutations on Anion Channel Activity

To investigate anion channel activity of Best1 mutants, we performed whole-cell patch clamp on HEK293 cells heterologously expressing Best1 or Best1 mutants fused to CFP or YFP (Fig. 4). We found, as we have previously,[10,17] that Best1-YFP (Fig. 4A) exhibits robust Cl^- currents in these cells compared to untransfected cells (controls) in the same plate. In contrast, currents for cells expressing Best1^{R141H}-YFP were significantly attenuated (Fig. 4A; $P < 0.03$) relative to Best1-YFP. Coexpression of Best1^{R141H}-YFP with Best1-CFP resulted in the rescue of channel activity, generating currents comparable with those observed in cells coexpressing Best1-CFP and Best1-YFP (Fig. 4B). Cells expressing Best1^{I366fsX18}-CFP exhibited currents that were significantly higher ($P < 0.05$) than cells expressing Best1-CFP (Fig. 4C). Cells coexpressing Best1^{I366fsX18}-CFP with Best1^{R141H}-YFP exhibited Cl^- currents comparable with cells coexpressing Best1-CFP and Best1-YFP (Fig. 4D).

Mean current at 100 mV was summarized for controls and each Best1 variant in Figure 4E. All cells expressing WT and/or mutant Best1 (Best1-CFP, Best1-YFP, Best1^{R141H}-YFP, Best1^{I366fsX18}-CFP, Best1-CFP + Best1-YFP, Best1^{R141H}-YFP + Best1-CFP, or Best1^{I366fsX18}-CFP + Best1^{R141H}-YFP) exhibited significantly higher ($p < 0.05$) currents than untransfected controls (Fig. 4E). Cells expressing Best1^{R141H}-YFP showed significantly ($p < 0.03$) reduced currents compared to Best1-YFP, while Best1^{I366fsX18}-CFP expressing cells showed significantly ($p < 0.05$) increased currents compared to Best1-CFP (Fig. 4E).

The expression of tagged Best1 and Best1 mutants in live HEK293 cells under patch clamp conditions is shown in Supplementary Figure S1. Best1-CFP, Best1-YFP, Best1^{R141H}-YFP, Best1^{I366fsX18}-CFP, Best1-CFP + Best1-YFP, Best1^{R141H}-YFP + Best1-CFP, and Best1^{I366fsX18}-CFP + Best1^{R141H}-YFP all exhibited comparable localization in transfected HEK293 cells (Supplementary Fig. S1). Although a large portion of transfected Best1 localized to intracellular compartments in transfected HEK293 cells, some Best1 appeared localized to the cell periphery (Supplementary Fig. S1). This localization pattern is consistent with what we have published in our previous work.[13] That each Best1 variant was tagged with CFP or YFP at its C-terminus was significant, as it was not uncommon to observe cells that did not comparably express both of the transfected Best1 variants (Supplementary Figs. S1H, S1I). Using differential tags allowed us to only patch cells comparably coexpressing both forms of tagged Best1 (Supplementary Figs. S1E–G).

Characterization of iPSC-RPE

We next sought to use iPSC-RPE as a primary cell culture model to further characterize the mutations identified in our presented patient. In addition to representing great therapeutic potential, iPSC-derived cells have proven to be very useful tools for understanding disease pathogenesis.[27,35] For these studies, we used an iPSC line (006-BIOTR-0001) obtained from the Mayo Clinic Center for Regenerative Medicine BioTrust. The successful generation of iPSCs from somatic skin fibroblasts was confirmed by the presence of the pluripotency markers Oct4, SSeA4, Nanog, Tra1-60, and Sox1 (Supplementary Figs. S2A–S2C). The induced pluripotent stem cells formed typical colonies in culture (Supplementary Fig. S2D) and maintained a normal karyotype (Supplementary Fig. S2E). As described in the methods, iPSCs were differentiated into iPSC-RPE using the method of Maruotti et al.[33] We grew iPSC-RPE cells to confluence in 60-mm dishes (Figs. 5A, 5B) or on permeable inserts (Corning, Inc.; Figs. 5C, 5D). The cells are densely packed with pigment granules (Figs. 5A–D) and exhibit the hexagonal, cobblestone appearance of typical RPE monolayers (Figs. 5B, 5D). Electron microscopy of iPSC-RPE grown on permeable inserts (Corning, Inc.) revealed dense apical microvilli and pigment granules (Fig. 5E). Examination at higher magnification identified a junctional complex at the apical lateral interface (Fig. 5F). Characteristic of RPE cells, no desmosomes were observed (Fig. 5F). As shown by immunoprecipitation and Western blotting, iPSC-RPE express the RPE differentiation markers Best1, CRALBP (Fig. 5G), and RPE65 (Fig. 5H). These induced pluripotent stem–RPE cells also efficiently phagocytose bovine photoreceptor outer segments at a rate comparable with that previously observed in other cells (Fig. 5I).[34] Measurements of transepithelial electrical resistances (TER) for cells grown on both permeable (Corning, Inc.) and Millicell HA filters (Millipore, Billerica, MA, USA) show that, within a few weeks, these cells generate an average TER of 159 ± 46 Ω*cm^2 (mean ± SD, $n = 132$). We have

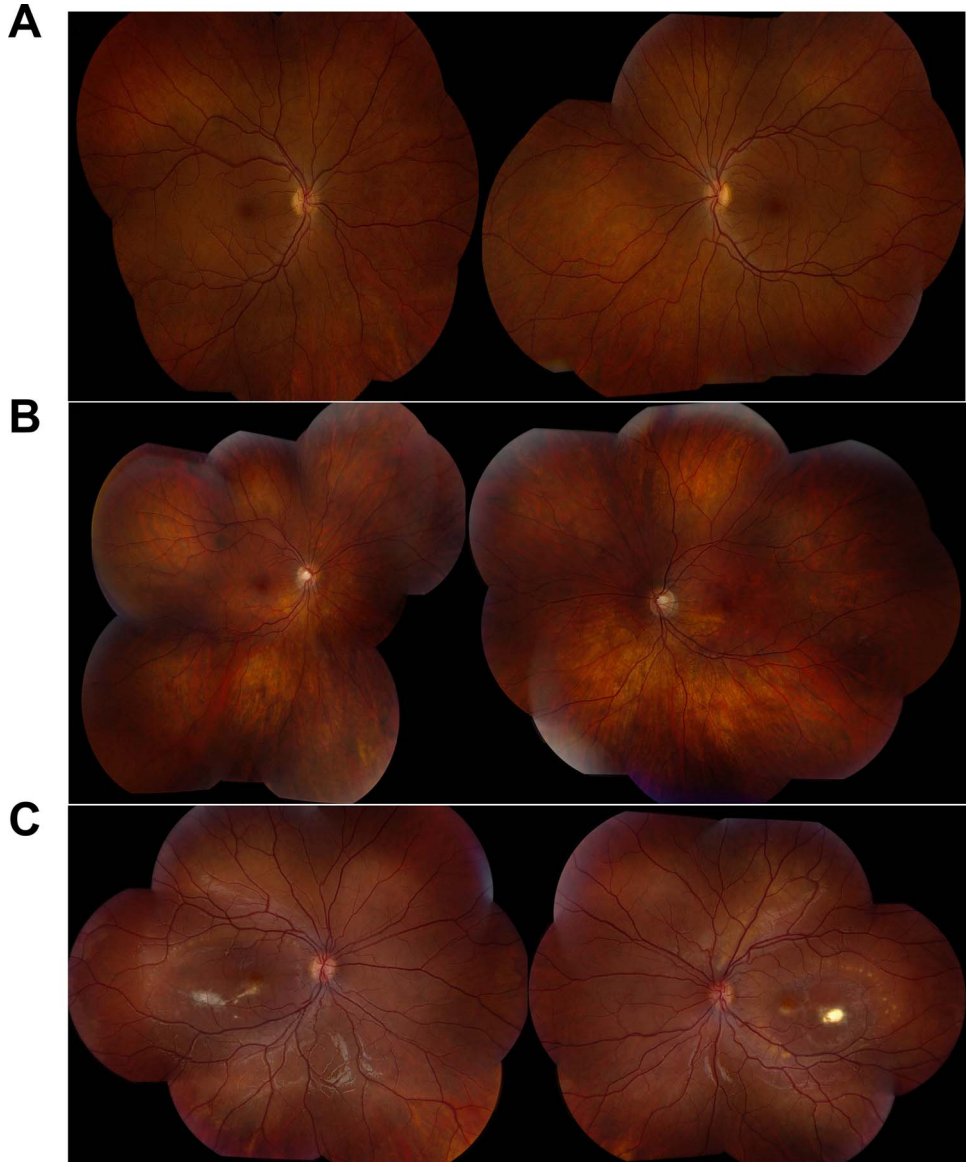

FIGURE 3. Fundus photos of the affected patient and the unaffected parents. No signs of retinal disease were observed in the patient's father (**A**) or mother (**B**). However, the patient (**C**), showed lesions predominantly localized to the macula. Left eye (*left panels*) and right eye (*right panels*).

observed TER as high as 1047 Ω*cm^2 for iPSC-RPE monolayers, though this is atypical. The combination of these data demonstrates the successful differentiation of iPSCs into RPE.

Best1^{I366fsX18} and Best1^{R141H} Are Properly Localized in RPE

We and others have previously shown that a large number of disease-causing mutations in *BEST1* disrupt protein trafficking.[10,11,31,36] Numerous ARB mutants are mislocalized in MDCK cells, though some exhibit proper localization to the basolateral plasma membrane.[10,36] Our iPSC-RPE form confluent and polarized monolayers which localize endogenous Best1 to the basolateral plasma membrane (Figs. 6A, 6B) and, as shown by ZO-1 staining, form tight junctions (Fig. 6). This is consistent with recent work published by Brandl et al.,[37] which found that endogenous Best1 was localized to the basolateral plasma membrane in iPSC-RPE. As we have found previously in fetal human RPE,[11,17] a portion of endogenous Best1 was also found in subapical intracellular compartments (Figs. 6A, 6B).

To further elucidate the potential role of mislocalization of Best1 in ARB, we expressed Best1-CFP, Best1$^{R141H-YFP}$, or Best1^{I366fsX18}-CFP in iPSC-RPE using adenovirus-mediated gene transfer and assessed localization via confocal X-Y and X-Z scans. Bestrophin 1–CFP localized to the plasma membrane in the X-Y (Fig. 6C) and X-Z (Fig. 6D) scans. Although Best1^{R141H} was previously found to be mislocalized in heterologous MDCK cells,[10,36] Best1^{R141H}-YFP was properly localized in iPSC-RPE in the presence of endogenous Best1 (Figs. 6E, 6F). Similarly, Best1^{I366fsX18}-CFP was found localized to the plasma membrane (Figs. 6G, 6H). Staining with ZO-1 highlighted the presence of tight junctions in each experiment and also served as a positional reference for the X-Y and X-Z scans (Fig. 6). Analogous to our previously published results using fetal human RPE,[11,17] a portion of overexpressed Best1 was found in subapical intracellular compartments (Figs. 6C–H).

The anti-Bestrophin-1 antibodies Pab-125 and E6-6 were generated in our laboratory to the same synthetic peptide, the

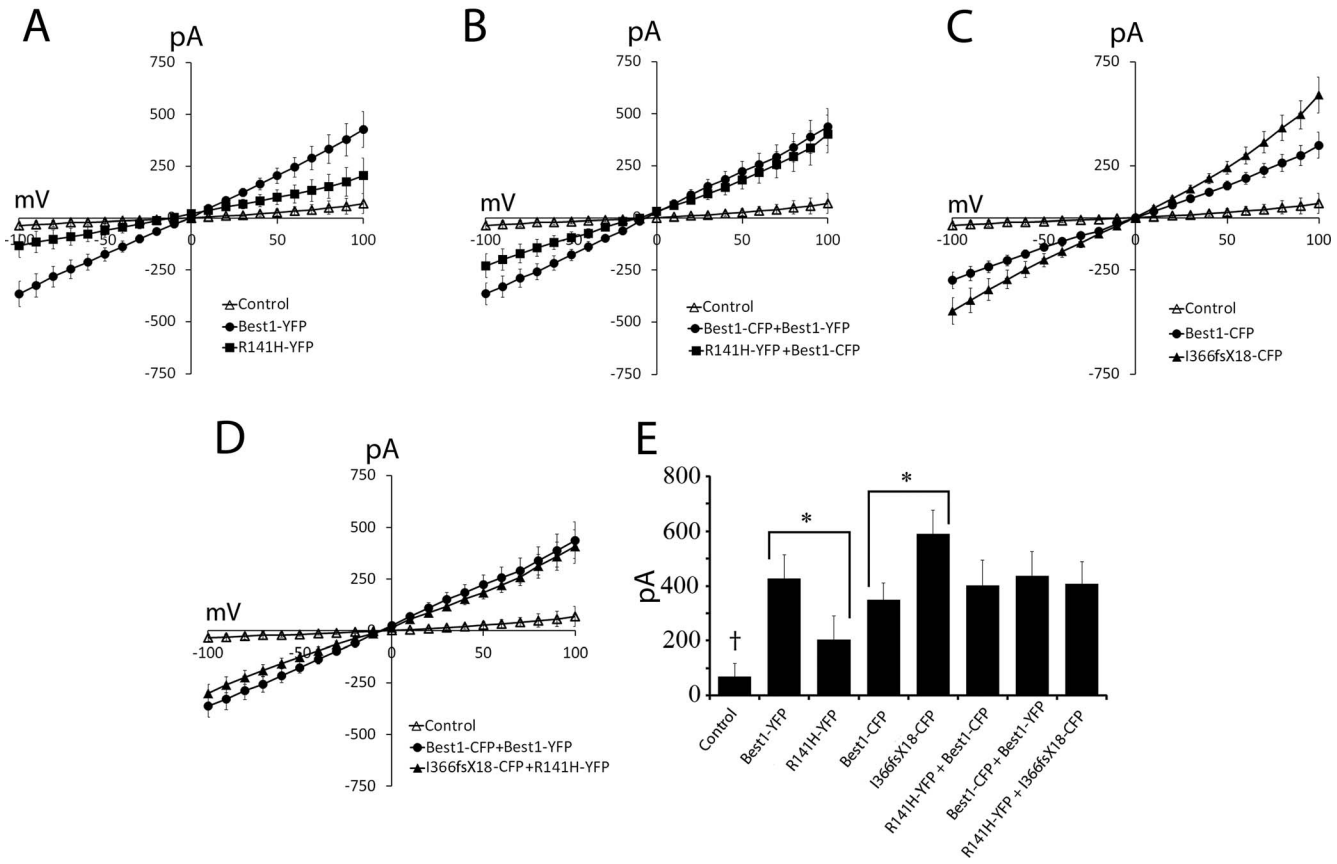

Figure 4. Whole-cell Cl^- currents of $Best1^{R141H}$, $Best1^{I366fsX18}$, and Best1 channels. (**A**) Whole-cell patch clamp was used to measure Cl^- currents in HEK293 cells transfected with Best1-YFP or $Best1^{R141H}$-YFP. Compared with Best1-YFP, $Best1^{R141H}$-YFP showed diminished Cl^- currents that were between those observed for Best1-YFP and untransfected controls. (**B**) Cells coexpressing Best1-CFP and $Best1^{R141H}$-YFP showed comparable currents to cells coexpressing Best1-CFP and Best1-YFP. (**C**) $Best1^{I366fsX18}$-CFP generated robust Cl^- currents that were significantly greater than that of Best1-CFP. (**D**) Coexpression of $Best1^{I366fsX18}$-CFP with $Best1^{R141H}$-YFP resulted in currents comparable to those generated by Best1-CFP and Best1-YFP. (**E**) Currents at +100 mV are summarized for each Best1 variant. All cells expressing a Best1 variant showed significantly higher currents than untransfected controls (indicated by the *dagger*). $Best1^{R141H}$-YFP showed significantly diminished currents compared with Best1-YFP, while $Best1^{I366fsX18}$-CFP showed significantly increased currents compared with Best1-CFP (indicated by *asterisks*). Data are presented as mean ± SD, $9 \leq n \leq 23$ for all experiments.

sequence of which corresponds to amino acids 566-585 of Best1.[6] This region comprises the carboxyl-terminus of the protein (Fig. 7A). Since the $Best1^{I366fsX18}$ mutant does not contain amino acids 367 through 585 of Best1 (Fig. 7A), neither of these antibodies can recognize $Best1^{I366fsX18}$-CFP. Taking advantage of this, we expressed $Best1^{I366fsX18}$-CFP in iPSC-RPE cells using adenovirus-mediated gene transfer. Mutant and endogenous Best1 were stained using antibodies specific to CFP or Best1, as described in the methods. Colocalization of $Best1^{I366fsX18}$-CFP and endogenous Best1 were then assessed using confocal microscopy. Consistent with Figure 6, we find that both $Best1^{I366fsX18}$-CFP and endogenous Best1 colocalize in the plasma membrane of iPSC-RPE cells (Fig. 7B).

WT Best1 and ARB Mutants as Well as Both ARB Mutants Interact With Each Other to Form Oligomers

Bestrophin 1 channels are comprised of homopentamers.[8,9] Our patch-clamp experiments suggest interaction between mutant and WT Best1 as well as between $Best1^{R141H}$-YFP and $Best1^{I366fsX18}$-CFP (Fig. 4). Moreover, our immunofluorescence data demonstrate that both $Best1^{I366fsX18}$-CFP and endogenous Best1 colocalize together (Fig. 7). These data (Figs. 4, 7) suggest that the different Best1 mutants can physically interact to form these homo-oligomers. To confirm this, we performed coimmunoprecipitation experiments between different forms of Best1.

We first tested this in iPSC-RPE cells. To assess oligomerization between different forms of Best1, iPSC-RPE cells were infected with Best1-YFP, $Best1^{R141H}$-YFP, or $Best1^{I366fsX18}$-CFP using adenovirus-mediated gene transfer. When these cells were immunoprecipitated for GFP and immunoblotted for Best1, bands corresponding to endogenous Best1 were found in all lanes except the control lane (Fig. 8A). Immunoblotting for Best1 identified fluorescently tagged forms of Best1 and $Best1^{R141H}$, but did not reveal $Best1^{I366fsX18}$-CFP because this truncation mutant lacks the epitope recognized by the antibody Pab-125.[6] A band corresponding to $Best1^{I366fsX18}$-CFP was also observed when infected cells were immunoprecipitated for Best1 and immunoblotted for GFP (Fig. 8B), demonstrating physical interaction between overexpressed mutant and endogenous Best1.

We next wanted to assess the ability of the two ARB mutants, $Best1^{R141H}$-YFP and $Best1^{I366fsX18}$-CFP, to interact with each other independent of endogenous Best1. We have previously shown that MDCK cells lack endogenous Best1 and that overexpressed Best1 forms homo-oligomers in this heterologous system.[10,11] Since endogenous Best1 would be a confounding factor for assessing oligomerization between

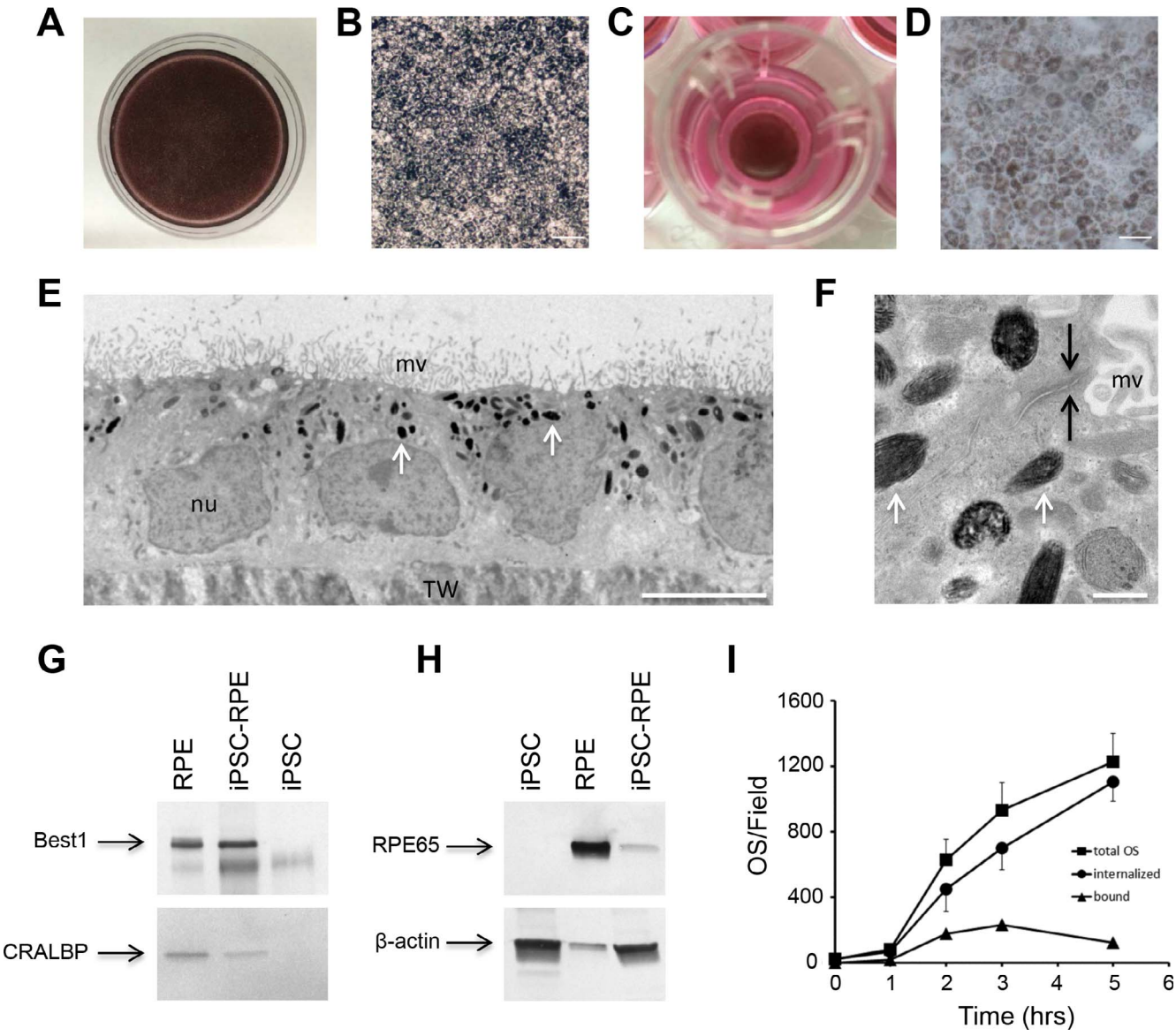

Figure 5. Characterization of iPSC-RPE. (**A**) Representative image of an iPSC-RPE monolayer grown to confluence in a 60-mm plate. (**B**) Higher magnification view of the hexagonal monolayer densely packed with pigment granules of such a plate. *Scale bar*: 50 μm. (**C**) Representative iPSC-RPE grown in a permeable insert (Corning, Inc.). (**D**) Higher magnification view of the hexagonal, pigment-dense monolayer of such a permeable insert (Corning, Inc.). *Scale bar*: 20 μm. (E) Transmission electron microscopy of iPSC-RPE grown on a permeable filter (Corning, Inc.) shows the presence of apical microvilli (mv) and pigment granules (indicated by *white arrows*). nu, nucleus; TW, Transwell filter. *Scale bar*: 5 μm. (**F**) Higher magnification of (**E**) shows a junctional complex (indicated by *black arrows*). *Scale bar*: 0.5 μm. (**G**) Immunoprecipitation and Western blotting demonstrates that, like RPE from a human donor eye (RPE) and unlike iPSCs, iPSC-RPE express Best1 and CRALBP. (**H**) Western blotting of iPSC, RPE, and iPSC-RPE lysates demonstrates expression of RPE65 in both RPE and iPSC-RPE. We used β-actin as the loading control. (**I**) Induced pluripotent stem–RPE cells grown in 96-well plates were incubated with FITC-labeled bovine outer segments (OS) for 0, 1, 2, 3, or 5 hours. Following quenching of bound but uninternalized OS fluorescence with trypan blue, total OS and internalized OS were determined and the number of bound OS calculated from the difference between total and internalized OS. Values are mean ± SD ($n > 4$).

Best1^{R141H} and Best1^{I366fsX18}, MDCK cells are an ideal system for studying mutant interaction independent of WT protein. We first demonstrated the utility of this system by showing that each ARB mutant is capable of physically interacting with overexpressed Best1-c-myc in MDCK cells. To do this, Best1-c-myc and Best1-YFP, Best1^{R141H}-YFP, or Best1^{I366fsX18}-CFP were coexpressed in confluent, polarized MDCK cells. When GFP was immunoprecipitated from lysates of coexpressing cells and immunoblotted for c-myc, bands were observed corresponding to Best1-c-myc in all lanes except the control lane (Fig. 8C). Bands for Best1-YFP, Best1^{R141H}-YFP, and Best1^{I366fsX18}-CFP were also observed when cells were immunoprecipitated for c-myc and immunoblotted for GFP (Fig. 8D), demonstrating reciprocal co-immunoprecipitation between WT and mutant Best1.

To assess interaction between each ARB mutant, MDCK cells were coinfected with both Best1^{R141H}-YFP and Best-1^{I366fsX18}-CFP. Coexpressing cells were immunoprecipitated for Best1^{R141H} using Pab-125, an antibody which recognizes Best1^{R141H} but not Best1^{I366fsX18}. Immunoprecipitation products were immunoblotted for GFP, revealing bands corresponding to both Best1^{R141H}-YFP and Best1^{I366fsX18}-CFP (Fig. 8E). Thus, Best1^{R141H} and Best1^{I366fsX18} are capable of physically interacting with the other.

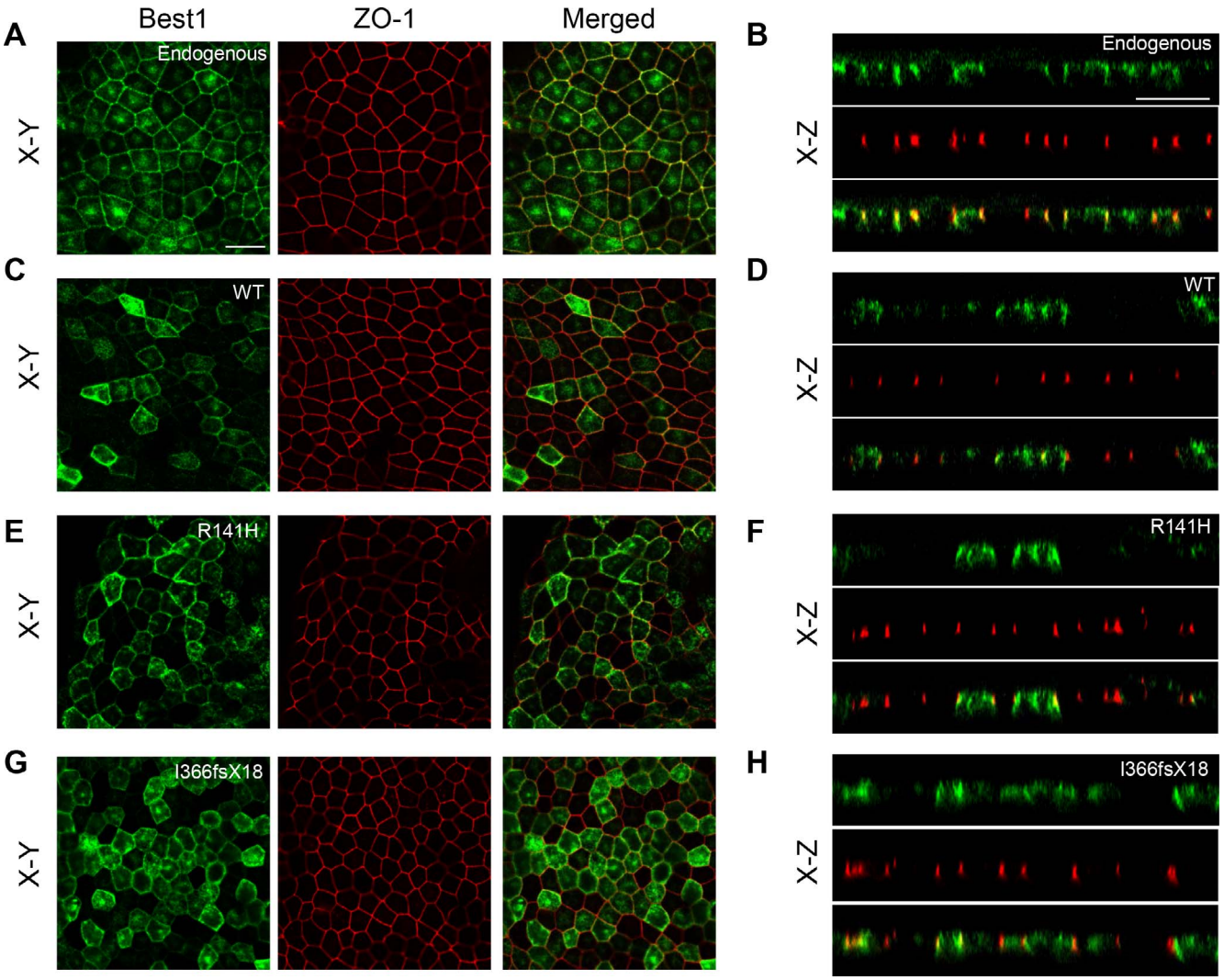

Figure 6. Endogenous Best1 as well as overexpressed Best1-YFP, Best1^{R141H}-YFP, and Best1^{I366fsX18}-CFP all localize to the plasma membrane in iPSC-RPE cells. Representative X-Y and X-Z scans of endogenous, overexpressed Best1, or overexpressed mutant Best1 (*green*) are shown with ZO-1 (*red*) as a positional marker. Mutants Best1 and Best1 were overexpressed using adenovirus-mediated transfer. Induced pluripotent stem–RPE cells exhibited tight junctions in the X-Y (**A**, **C**, **E**, **G**) and X-Z scans (**B**, **D**, **F**, **H**). Endogenous Best1 was localized to the basolateral plasma membrane (**A**, **B**). Overexpressed Best1-CFP (**C**, **D**), Best1^{R141H}-YFP (**E**, **F**), and Best1^{I366fsX18}-CFP (**G**, **H**) were also localized to the basolateral plasma membrane. *Scale bar*: 20 μM.

Discussion

In this study, we describe a young female patient with ARB due to compound heterozygous mutations in *BEST1*. The mutation R141H has been previously reported in association with ARB.[3,32] The other mutation, I366fsX18, has not previously been described. In addition to decreased visual acuity and a depressed EOG, the patient exhibited classical symptoms of ARB as revealed by fundus photography (Figs. 1, 3C) and OCT (Fig. 2) imaging. Abnormally long photoreceptor outer segments were observed in both of the subject's eyes (Fig. 2), though this was especially pronounced in the right eye (Fig. 2A). This is of note because patients with BVMD also display elongated outer segments and increased outer segment equivalent lengths.[38,39]

Compared with cells expressing Best1-CFP, cells expressing Best1^{I366fsX18}-CFP showed larger Cl^- currents in HEK293 cells (Fig. 4C). Since Best1^{I366fsX18} spans the intracellular N-terminus and all four transmembrane domains yet lacks the bulk of the cytosolic C-terminus (Fig. 7A), this indicates that the first 366 amino acids are sufficient for Best1's channel function. That Best1^{I366fsX18}-CFP lacks this region and exhibited larger currents than Best1-CFP (Fig. 4C) indicates that the latter 219 amino acids of Best1 may play an inhibitory role in regulating Best1 channel activity. This is similar to what has been observed for mouse bestrophin-3, which contains a C-terminal motif that inhibits its channel function.[40] The carboxyl terminal cytoplasmic domain of Best1 is sensitive to phosphorylation and interacts with protein phosphatase 2A.[41] This carboxyl terminal region also mediates functional and physical interaction with voltage dependent Ca^{2+} channels.[16,42] Thus, the amino acid residues which the Best1^{I366fsX18} mutant lacks may regulate channel activity through changes in phosphorylation and/or calcium homeostasis.

As was previously reported by Burgess et al.,[3] we find that the R141H mutation attenuates Best1 Cl^- currents (Fig. 4A) and that coexpression with Best1 results in a rescue of channel activity, generating currents comparable to Best1-CFP and Best1-YFP (Fig. 4B). This is corroborative of work by Davidson et al.,[36] which identified ARB mutants that failed to suppress

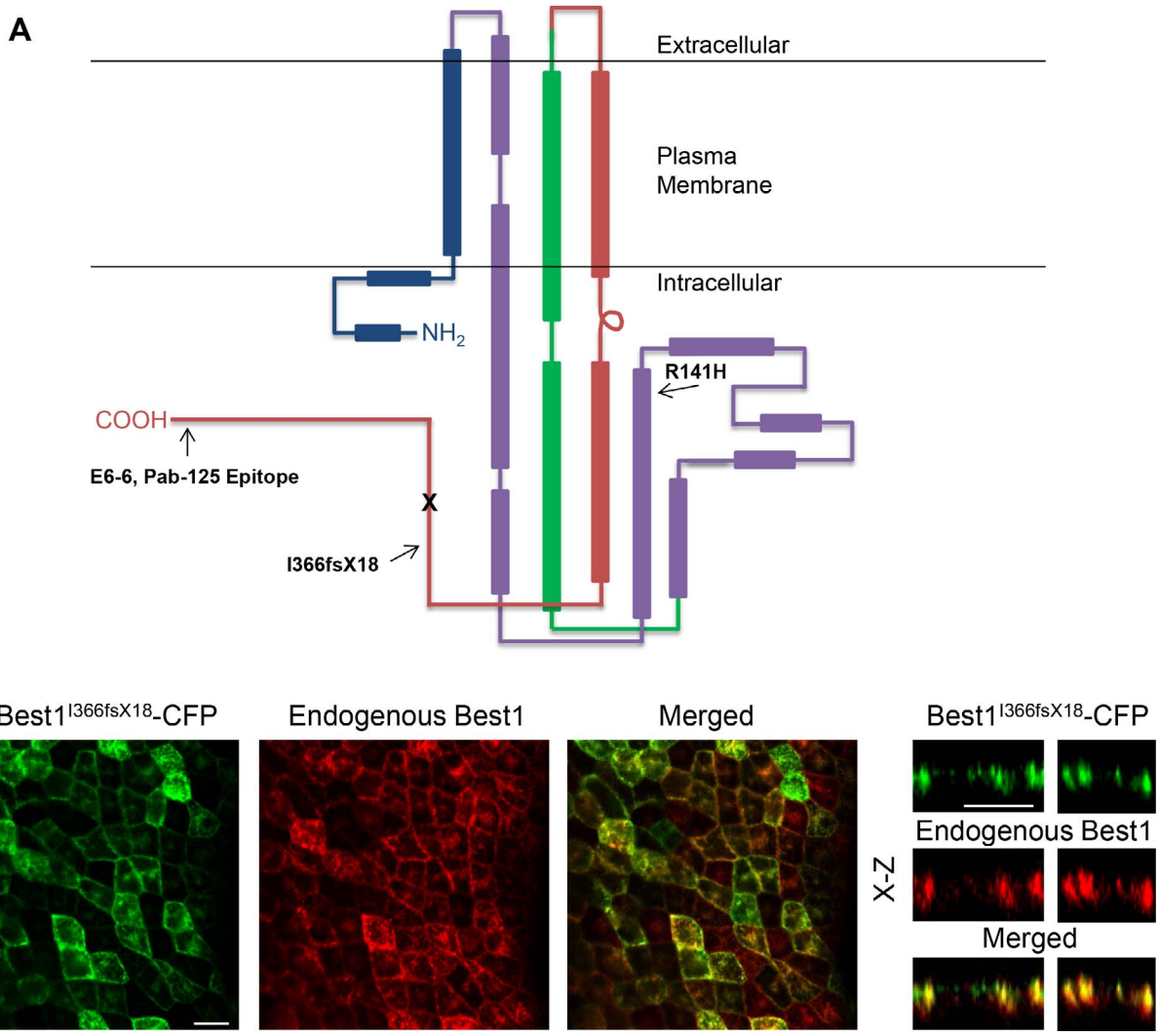

Figure 7. Best1^{I366fsX18}-CFP colocalizes with endogenous Best1 in iPSC-RPE cells. (**A**) Assumed topology of a Best1 monomer in the plasma membrane, based on the crystal structure data of chicken Best1. The mutation site of R141H is located in the cytosolic loop between transmembrane domains 2 and 3. The mutation site of I366fsX18 is located in the cytosolic C-terminal domain and results in a premature stop codon at position 383, indicated by the *X*. Our two anti-Best1 antibodies, E6-6 and Pab-125, both recognize an epitope comprised of the last 18 amino acids of Best1 which are not present in the Best1^{I366fsX18} mutant. (**B**) Bestrophin 1^{I366fsX18}-CFP was overexpressed in iPSC-RPE cells using adenovirus-mediated gene transfer. Induced pluripotent stem–RPE cells were stained using an antibody against endogenous Best1 (*red*) and an antibody against CFP (*green*). As assessed by confocal X-Y and X-Z scans, both Best1^{I366fsX18}-CFP and endogenous Best1 colocalize together in the plasma membrane. *Scale bars*: 20 μM for the X-Y scan and 10 μM for the X-Z scan.

currents of Best1 in co-expressing HEK293 cells. It was previously reported that, in mouse Bestrophin-2, the mutation R141C results in altered, but not suppressed, currents in transfected HEK293 cells.[43] The best interpretation of this difference is that substitution with cysteine is more benign than substitution with histidine with regards to channel activity. Position R141 is located in the cytosolic loop between transmembrane domains 2 and 3 (Fig. 7A) and, based on crystal structure data from bacterial and chicken Best1,[8,9] is not part of the channel pore. The R141H mutation may therefore disrupt channel activity by disrupting an amino acid signal important for Best1 regulation.

Our patch clamp data for Best1^{R141H} and Best1^{I366fsX18} stand in stark contrast to other BVMD mutants which, when coexpressed with Best1, invariably suppress the current of WT protein.[15,16] It was previously reported by Davidson et al.[36] that, when coexpressed together in HEK293 cells, the ARB mutants Best1^{D312N} and Best1^{M325T} exhibit significantly attenuated channel activity. Similarly, the ARB mutant pair Best1^{R141H} and Best1^{V317M} displayed abrogated Cl^- currents in transfected HEK293 cells.[36] In contrast, we find that coexpression of Best1^{R141H}-YFP and Best1^{I366fsX18}-CFP results in Cl^- currents comparable with cells coexpressing Best1-CFP and Best1-YFP (Fig. 4D). Given this and that the combinations of Best1^{R141H} and Best1 as well as Best1^{R141H} and Best1^{I366fsX18} both result in robust Cl^- currents, yet only the latter combination causes disease (Fig. 3), this suggests that loss of Cl^- channel activity is not a contributing factor for this patient's disease. More broadly, ARB may differ from BVMD in that loss of channel activity is not a major contributory factor to disease pathogenesis. This may also vary from patient to patient, however, as some ARB mutant pairs in combination exhibit lower channel activity than each ARB mutant alone or each ARB mutant in combination with WT Best1.[36]

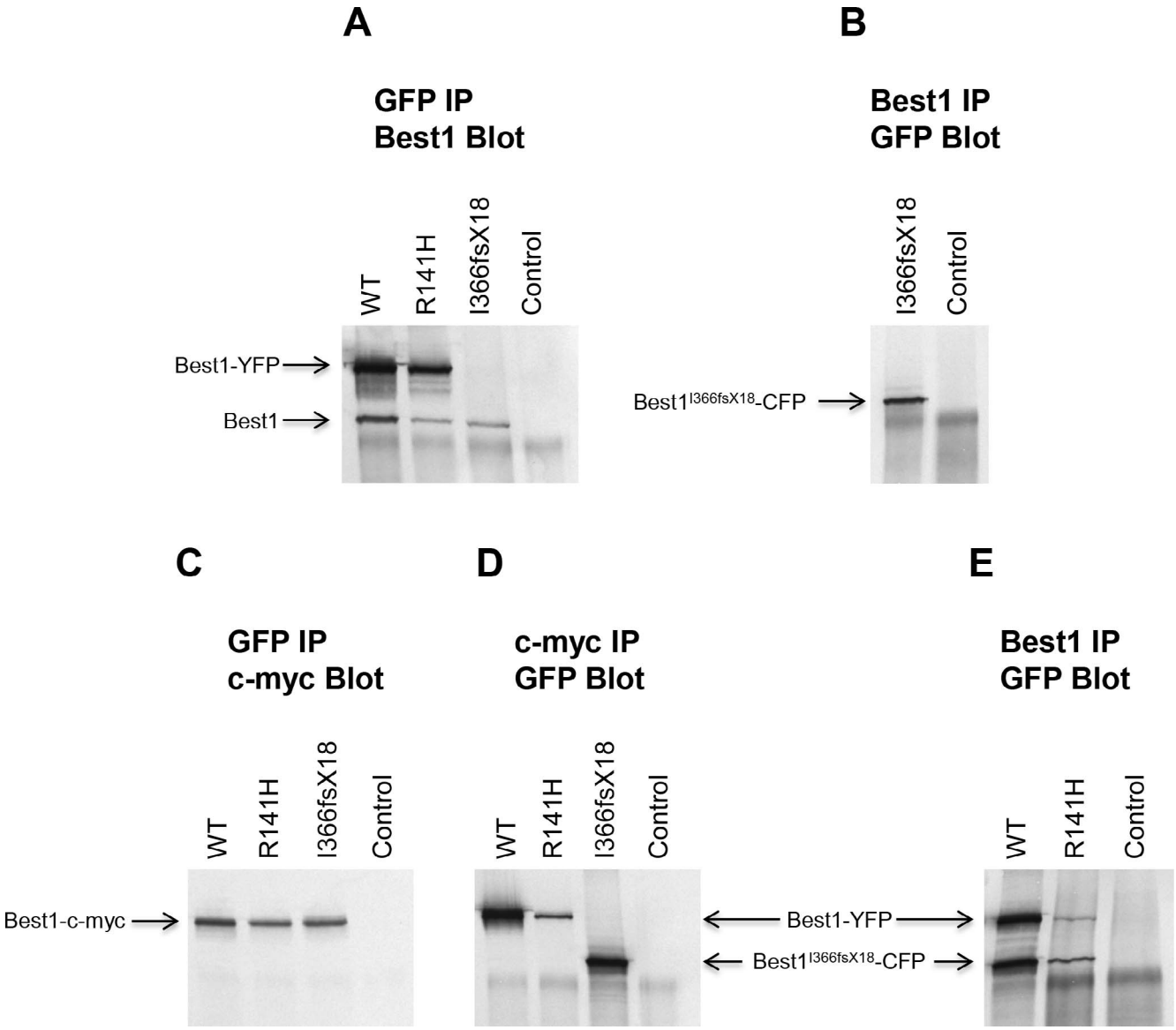

Figure 8. Best1^{R141H} and Best1^{I366fsX18} coimmunoprecipitate with each other as well as endogenous and overexpressed Best1. (**A**) Bestrophin 1-YFP, Best1^{R141H}-YFP, and Best1^{I366fsX18}-CFP were all overexpressed in iPSC-RPE using adenovirus-mediated gene transfer. Induced pluripotent stem–RPE cells were immunoprecipitated (IPed) using an anti-GFP antibody (which recognizes CFP and YFP) and immunoblotted for Best1. (**B**) Bestrophin 1^{I366fsX18}-CFP was overexpressed in iPSC-RPE and iPSC-RPE were IPed for Best1 using an antibody that recognizes an epitope the Best1^{I366fsX18} mutant lacks. Induced pluripotent stem–RPE cells were then immunoblotted for GFP. (**C**, **D**) Madin-Darby canine kidney II cells were coinfected with Best1-c-myc and Best1-YFP, Best1^{R141H}-YFP, or Best1^{I366fsX18}-CFP. Cells were then IPed for GFP (**C**) or c-myc (**D**) and immunoblotted for c-myc (**C**) or GFP (**D**). (**E**) Madin-Darby canine kidney II cells were coinfected with Best1^{I366fsX18}-CFP and either Best1-YFP or Best1^{R141H}-YFP. Cells were IPed for Best1 using an antibody which doesn't recognize the Best1^{I366fsX18} mutant and then immunoblotted for GFP.

We show that the novel Best1^{I366fsX18} mutant co-localizes (Fig. 7B) and reciprocally coimmunoprecipitates with endogenous Best1 in iPSC-RPE cells (Figs. 8A, 8B). Bestrophin 1^{R141H} coimmunoprecipitates with endogenous Best1 in iPSC-RPE cells (Fig. 8A) and Best1^{R141H} and Best1^{I366fsX18} coimmunoprecipitate with each other in MDCK cells (Fig. 8E). This demonstrates that the first 366 amino acids of Best1 are sufficient to mediate homo-oligomerization. This is the first time that a Best1 mutant has been shown to physically interact with endogenous Best1 in a native system and also the first time that two ARB mutants have been shown to physically interact with each other. Previous oligomerization[10,12] and crystal structure data[8,9] have demonstrated that the C-terminus does not play a cogent role in the formation of homo-oligomers. Our patch clamp (Fig. 4) and oligomerization data (Figs. 7, 8) for the Best1^{I366fsX18} mutant, which contains all four transmembrane domains yet lacks the bulk of the cytosolic C-terminus (Fig. 7A), confirms these structural findings.

With regard to trafficking, both Best1^{R141H} and Best-1^{I366fsX18} were properly localized to the plasma membrane in iPSC-RPE (Figs. 6E–H). As before with the channel activity and homo-oligomerization findings, this demonstrates that the first 366 amino acids are sufficient to mediate proper localization in the presence of endogenous Best1. Interestingly, we and another group previously found that Best1^{R141H} was mislocalized to intracellular compartments in MDCK cells.[10,36] When coexpressed with Best1 in MDCK cells, Best1^{R141H} was shown to predominantly colocalize with Best1 in internal compartments, though some co-localization was observed at the cell periphery.[10] Since Best1 localizes to the basolateral plasma

membrane in MDCK cells, this heterologous system has been shown to be efficacious at highlighting trafficking differences of Best1 mutants independent of WT Best1.[10,11,31,36,44] However, given that Best1^{R141H} was properly localized in the presence of endogenous Best1 in iPSC-RPE (Figs. 6E, 6F) and yet predominantly mislocalized when coexpressed with Best1 in MDCK cells,[10] this would suggest that mislocalization in MDCK cells should be verified in iPSC-RPE or another RPE cell culture model.

A single copy of either the R141H or I366fsX18 mutation does not result in retinal disease (Figs. 3A, 3B), while the combination of the I366fsX18 and R141H mutations results in ARB (Figs. 1, 2, 3C). Unlike Best1, Best1^{I366fsX18} is missing amino acids 383 through 585 and, due to the frame-shift inducing deletion, amino acids 367 through 382 are nonsensical. Thus, this mutant is comprised only of the first 366 amino acids of normal Best1. Somehow, the truncation of this region results in the difference between a healthy retina in the father heterozygous for the R141H mutation (Fig. 3A) and a diseased retina in the patient compound heterozygous for R141H and I366fsX18 (Figs. 1, 2, 3C). The carboxyl terminus appears to be necessary for overcoming the defect caused by the R141H mutation, as its presence in the father heterozygous for the R141H mutation does not result in disease (Fig. 3A). This carboxyl terminal region may hold the key to understanding the pathogenesis of ARB, and future studies should investigate why and how the loss of this region may lead to retinal dysfunction. Since the C-terminus has been shown to play roles in the regulation and interaction of voltage dependent Ca^{2+} channels,[25,42,45,46] the Best1^{I366fsX18} mutant may impair Ca^{2+} homeostasis.

Extreme heterogeneity has been previously documented in patients harboring BVMD mutations. Within the same family harboring the same known dominant mutation, substantial variability in vision loss, fundus presentation, and age of disease onset has been reported.[4,5] Some 7% to 9% of all patients harboring BVMD mutations are, aside from a decreased Arden ratio in the EOG, clinically asymptomatic.[4,5] As such, any *BEST1* mutation that appears recessive may in actuality be an asymptomatic presentation of a BVMD mutation. However, this is unlikely to be the case in this study for the following reasons:

1. The mutation R141H has been previously reported to be recessive by two different groups.[3,32]
2. The novel mutation I366fsX18 is similar to previously reported recessive, truncation mutations associated with ARB.[3,47–49]
3. In the presented family, these mutations exhibit a clear mode of autosomal recessive inheritance (Fig. 3).

In addition to identifying a novel ARB mutation, our data presented herein provide significant insights into the pathogenesis of ARB as well as the protein regions governing Best1 channel activity, co-trafficking, and homo-oligomerization. They also further demonstrate the utility of employing iPSC-RPE as a primary cell culture model for better understanding the mechanisms underlying retinal disease.

Acknowledgments

Supported by the NIH Grants EY13160 (ADM) and EY014465 (LYM); Research to Prevent Blindness (unrestricted grant to the Department of Ophthalmology at the Mayo Clinic in Rochester, MN, USA); a gift to the Mayo Clinic Center for Regenerative Medicine from Eugene Wood; and a gift from the Deshong family.

Disclosure: **A.A. Johnson**, None; **L.A. Bachman**, None; **B.J. Gilles**, None; **S.D. Cross**, None; **K.E. Stelzig**, None; **Z.T. Resch**, None; **L.Y. Marmorstein**, None; **J.S. Pulido**, None; **A.D. Marmorstein**, None

References

1. Petrukhin K, Koisti MJ, Bakall B, et al. Identification of the gene responsible for Best macular dystrophy. *Nat Genet*. 1998; 19:241–247.
2. Marquardt A, Stohr H, Passmore LA, Kramer F, Rivera A, Weber BH. Mutations in a novel gene, VMD2, encoding a protein of unknown properties cause juvenile-onset vitelliform macular dystrophy (Best's disease). *Hum Mol Genet*. 1998;7:1517–1525.
3. Burgess R, Millar ID, Leroy BP, et al. Biallelic mutation of BEST1 causes a distinct retinopathy in humans. *Am J Hum Genet*. 2008;82:19–31.
4. Marmorstein AD, Cross HE, Peachey NS. Functional roles of bestrophins in ocular epithelia. *Prog Retin Eye Res*. 2009;28: 206–226.
5. Boon CJ, Klevering BJ, Leroy BP, Hoyng CB, Keunen JE, den Hollander AI. The spectrum of ocular phenotypes caused by mutations in the BEST1 gene. *Prog Retin Eye Res*. 2009;28: 187–205.
6. Marmorstein AD, Marmorstein LY, Rayborn M, Wang X, Hollyfield JG, Petrukhin K. Bestrophin, the product of the Best vitelliform macular dystrophy gene (VMD2), localizes to the basolateral plasma membrane of the retinal pigment epithelium. *Proc Natl Acad Sci U S A*. 2000;97:12758–12763.
7. Milenkovic VM, Rivera A, Horling F, Weber BH. Insertion and topology of normal and mutant bestrophin-1 in the endoplasmic reticulum membrane. *J Biol Chem*. 2007;282:1313–1321.
8. Dickson VK, Pedi L, Long SB. Structure and insights into the function of a Ca-activated Cl channel. *Nature*. 2014;516:213–218.
9. Yang T, Liu Q, Kloss B, et al. Structure and selectivity in bestrophin ion channels. *Science*. 2014;346:355–359.
10. Johnson AA, Lee YS, Chadburn AJ, et al. Disease-causing mutations associated with four bestrophinopathies exhibit disparate effects on the localization, but not the oligomerization, of Bestrophin-1. *Exp Eye Res*. 2014;121:74–85.
11. Johnson AA, Lee YS, Stanton JB, et al. Differential effects of Best disease causing missense mutations on bestrophin-1 trafficking. *Hum Mol Genet*. 2013;22:4688–4697.
12. Sun H, Tsunenari T, Yau KW, Nathans J. The vitelliform macular dystrophy protein defines a new family of chloride channels. *Proc Natl Acad Sci U S A*. 2002;99:4008–4013.
13. Stanton JB, Goldberg AF, Hoppe G, Marmorstein LY, Marmorstein AD. Hydrodynamic properties of porcine bestrophin-1 in Triton X-100. *Biochim Biophys Acta*. 2006;1758:241–247.
14. Bharill S, Fu Z, Palty R, Isacoff EY. Stoichiometry and specific assembly of Best ion channels. *Proc Natl Acad Sci U S A*. 2014; 111:6491–6496.
15. Hartzell HC, Qu Z, Yu K, Xiao Q, Chien LT. Molecular physiology of bestrophins: multifunctional membrane proteins linked to best disease and other retinopathies. *Physiol Rev*. 2008;88:639–672.
16. Xiao Q, Hartzell HC, Yu K. Bestrophins and retinopathies. *Pflugers Arch*. 2010;460:559–569.
17. Marmorstein AD, Kinnick TR, Stanton JB, Johnson AA, Lynch RM, Marmorstein LY. Bestrophin-1 influences transepithelial electrical properties and Ca(2+) signaling in human retinal pigment epithelium. *Mol Vis*. 2015;21:347–359.
18. Milenkovic A, Brandl C, Milenkovic VM, et al. Bestrophin 1 is indispensable for volume regulation in human retinal pigment

epithelium cells. *Proc Natl Acad Sci U S A*. 2015;112:E2630–E2639.

19. Lee S, Yoon BE, Berglund K, et al. Channel-mediated tonic GABA release from glia. *Science*. 2010;330:790–796.
20. Woo DH, Han KS, Shim JW, et al. TREK-1 and Best1 channels mediate fast and slow glutamate release in astrocytes upon GPCR activation. *Cell*. 2012;151:25–40.
21. Yu K, Lujan R, Marmorstein A, Gabriel S, Hartzell HC. Bestrophin-2 mediates bicarbonate transport by goblet cells in mouse colon. *J Clin Invest*. 2010;120:1722–1735.
22. Cui CY, Childress V, Piao Y, et al. Forkhead transcription factor FoxA1 regulates sweat secretion through Bestrophin 2 anion channel and Na-K-Cl cotransporter 1. *Proc Natl Acad Sci U S A*. 2012;109:1199–1203.
23. Marmorstein LY, Wu J, McLaughlin P, et al. The light peak of the electroretinogram is dependent on voltage-gated calcium channels and antagonized by bestrophin (best-1). *J Gen Physiol*. 2006;127:577–589.
24. Rosenthal R, Bakall B, Kinnick T, et al. Expression of bestrophin-1, the product of the VMD2 gene, modulates voltage-dependent Ca2+ channels in retinal pigment epithelial cells. *FASEB J*. 2006;20:178–180.
25. Yu K, Xiao Q, Cui G, Lee A, Hartzell HC. The best disease-linked Cl- channel hBest1 regulates Ca V 1 (L-type) Ca2+ channels via src-homology-binding domains. *J Neurosci*. 2008; 28:5660–5670.
26. Zhang Y, Stanton JB, Wu J, et al. Suppression of Ca2+ signaling in a mouse model of Best disease. *Hum Mol Genet*. 2010;19: 1108–1118.
27. Singh R, Shen W, Kuai D, et al. iPS cell modeling of Best disease: insights into the pathophysiology of an inherited macular degeneration. *Hum Mol Genet*. 2013;22:593–607.
28. Gomez NM, Tamm ER, Straubeta O. Role of bestrophin-1 in store-operated calcium entry in retinal pigment epithelium. *Pflugers Arch*. 2013;465:481–495.
29. Neussert R, Muller C, Milenkovic VM, Strauss O. The presence of bestrophin-1 modulates the Ca2+ recruitment from Ca2+ stores in the ER. *Pflugers Arch*. 2010;460:163–175.
30. Strauss O, Muller C, Reichhart N, Tamm ER, Gomez NM. The role of bestrophin-1 in intracellular Ca(2+) signaling. *Adv Exp Med Biol*. 2014;801:113–119.
31. Milenkovic VM, Rohrl E, Weber BH, Strauss O. Disease-associated missense mutations in bestrophin-1 affect cellular trafficking and anion conductance. *J Cell Sci*. 2011;124:2988–2996.
32. Iannaccone A, Kerr NC, Kinnick TR, Calzada JI, Stone EM. Autosomal recessive best vitelliform macular dystrophy: report of a family and management of early-onset neovascular complications. *Arch Ophthalmol*. 2011;129:211–217.
33. Maruotti J, Wahlin K, Gorrell D, Bhutto I, Lutty G, Zack DJ. A simple and scalable process for the differentiation of retinal pigment epithelium from human pluripotent stem cells. *Stem Cells Transl Med*. 2013;2:341–354.
34. Finnemann SC, Bonilha VL, Marmorstein AD, Rodriguez-Boulan E. Phagocytosis of rod outer segments by retinal pigment epithelial cells requires alpha(v)beta5 integrin for binding but not for internalization. *Proc Natl Acad Sci U S A*. 1997;94:12932–12937.
35. Rohani L, Johnson AA, Arnold A, Stolzing A. The aging signature: a hallmark of induced pluripotent stem cells? *Aging Cell*. 2014;13:2–7.
36. Davidson AE, Millar ID, Burgess-Mullan R, et al. Functional characterization of bestrophin-1 missense mutations associated with autosomal recessive bestrophinopathy. *Invest Ophthalmol Vis Sci*. 2011;52:3730–3736.
37. Brandl C, Zimmermann SJ, Milenkovic VM, et al. In-depth characterisation of retinal pigment epithelium (RPE) cells derived from human induced pluripotent stem cells (hiPSC). *Neuromolecular Med*. 2014;16:551–564.
38. Abramoff MD, Mullins RF, Lee K, et al. Human photoreceptor outer segments shorten during light adaptation. *Invest Ophthalmol Vis Sci*. 2013;54:3721–3728.
39. Kay CN, Abramoff MD, Mullins RF, et al. Three-dimensional distribution of the vitelliform lesion, photoreceptors, and retinal pigment epithelium in the macula of patients with best vitelliform macular dystrophy. *Arch Ophthalmol*. 2012;130: 357–364.
40. Qu Z, Cui Y, Hartzell C. A short motif in the C-terminus of mouse bestrophin 3 [corrected] inhibits its activation as a Cl channel. *FEBS Lett*. 2006;580:2141–2146.
41. Marmorstein LY, McLaughlin PJ, Stanton JB, Yan L, Crabb JW, Marmorstein AD. Bestrophin interacts physically and functionally with protein phosphatase 2A. *J Biol Chem*. 2002;277: 30591–30597.
42. Xiao Q, Prussia A, Yu K, Cui YY, Hartzell HC. Regulation of bestrophin Cl channels by calcium: role of the C terminus. *J Gen Physiol*. 2008;132:681–692.
43. Qu Z, Chien LT, Cui Y, Hartzell HC. The anion-selective pore of the bestrophins, a family of chloride channels associated with retinal degeneration. *J Neurosci*. 2006;26:5411–5419.
44. Davidson AE, Millar ID, Urquhart JE, et al. Missense mutations in a retinal pigment epithelium protein, bestrophin-1, cause retinitis pigmentosa. *Am J Hum Genet*. 2009;85:581–592.
45. Reichhart N, Milenkovic VM, Halsband CA, Cordeiro S, Strauss O. Effect of bestrophin-1 on L-type Ca2+ channel activity depends on the Ca2+ channel beta-subunit. *Exp Eye Res*. 2010;91:630–639.
46. Milenkovic VM, Krejcova S, Reichhart N, Wagner A, Strauss O. Interaction of bestrophin-1 and Ca2+ channel beta-subunits: identification of new binding domains on the bestrophin-1 C-terminus. *PLoS One*. 2011;6:e19364.
47. Pomares E, Bures-Jelstrup A, Ruiz-Nogales S, Corcostegui B, Gonzalez-Duarte R, Navarro R. Nonsense-mediated decay as the molecular cause for autosomal recessive bestrophinopathy in two unrelated families. *Invest Ophthalmol Vis Sci*. 2012;53: 532–537.
48. Bitner H, Mizrahi-Meissonnier L, Griefner G, Erdinest I, Sharon D, Banin E. A homozygous frameshift mutation in BEST1 causes the classical form of Best disease in an autosomal recessive mode. *Invest Ophthalmol Vis Sci*. 2011;52:5332–5338.
49. Davidson AE, Sergouniotis PI, Burgess-Mullan R, et al. A synonymous codon variant in two patients with autosomal recessive bestrophinopathy alters in vitro splicing of BEST1. *Mol Vis*. 2010;16:2916–2922.

Investigative Ophthalmology & Visual Science